Talanta 89 (2012) 417–421

Contents lists available at SciVerse ScienceDirect

Talanta

journal homepage: www.elsevier.com/locate/talanta

Enhanced nonenzymatic hydrogen peroxide sensing with reduced graphene oxide/ferroferric oxide nanocomposites

Yiping Ye[a], Tao Kong[b,*], Xiaofang Yu[c], Yukun Wu[c], Kun Zhang[c], Xiaoping Wang[a,c,**]

[a] Department of Physics, University of Science and Technology of China, Hefei, Anhui 230026, PR China
[b] Suzhou Institute of Nano-Tech and Nano-Bionics, Chinese Academy of Sciences, Suzhou, Jiangsu 215123, PR China
[c] Hefei National Laboratory for Physical Sciences at the Microscale, University of Science and Technology of China, Hefei, Anhui 230026, PR China

ARTICLE INFO

Article history:
Received 10 August 2011
Received in revised form
19 December 2011
Accepted 19 December 2011
Available online 24 December 2011

Keywords:
Reduced graphene oxide
Ferroferric oxide
Nanocomposite
Hydrogen peroxide sensor
Nonenzymatic

ABSTRACT

A nonenzymatic hydrogen peroxide (H_2O_2) sensor was fabricated using the reduced graphene oxide (RGO) and ferroferric oxide (Fe_3O_4) nanocomposites as the sensing material. The nanocomposites were synthesized by coprecipitation method and characterized by high-resolution transmission electron microscopy and X-ray diffraction. Results showed that the RGO sheet was evenly decorated by the well-crystallized Fe_3O_4 nanoparticles. The nanocomposites showed enhanced catalytic ability to the reduction of hydrogen peroxide compared with the RGO, Fe_3O_4 nanoparticles alone and the mixture materials. The sensor has a quite wide linear range from 0.1 mM to 6 mM (R^2 = 0.990) with less than 5 s response time. Moreover, its detection limit is 3.2 μM (S/N = 3). The anti-interference ability, long-term stability and potential application in real samples of the sensor is also assessed. This work expands the application of the graphene-based nanomaterials in the sensor areas.

1. Introduction

The fast and accurate detection of hydrogen peroxide (H_2O_2) has profound applications in pharmaceutical, clinical, food industry, environmental analysis and other fields. Numerous methods have been applied for the detection of H_2O_2, such as fluorometry [1], chemiluminescence [2], and electrochemical methods [3]. Among these methods, the electrochemical method is most studied because of its simplicity and fast response for analysis. Generally, the electro-oxidation or electro-reduction of H_2O_2 on bare gold or the carbon electrode which are extensively used in the electrochemical experiments requires high overpotential, while common electroactive species will confuse the measurements. Under this circumstance, it is a great interest to fabricate chemically modified electrodes for the detection of H_2O_2 with high efficiency and selectivity. Most of these methods are based on the immobilization of enzymes such as horseradish peroxidase [4], cytochrome *c* [5] and myoglobin [6] on the functionalized electrodes. Although the enzyme based biosensors can acquire remarkable selectivity, they usually suffer from the complicated enzyme immobilization processes and the instability of the immobilized biomolecules. Thus, the nonenzymatic sensor for the detection of H_2O_2 is great appreciated to current researchers.

Magnetic materials have been attracted more and more concerns in recent years [7,8] because of their potential in biomarker [9], medical imaging [10,11] and drug delivery [12]. In the biosensor field, Gao et al. [13] reported that ferromagnetic nanoparticles had intrinsic enzyme mimetic activity similar to that found in common peroxidases. Since then, lots of groups explored the catalytic effect of Fe_3O_4 nanoparticles to hydrogen peroxide using various methods, such as spectroscopy [14] and electrochemical method [15]. However, due to the high specific surface area and large interaction of magnetic dipole, magnetic nanoparticles are tended to be highly aggregated. Moreover, biosensors constructed with Fe_3O_4 nanoparticles usually shows poor performance with low sensitivity and narrow linear range [16]. In this regards, proper and effective surface modification are highly desired to overcome these limitations [17].

Due to the excellent electrical, mechanical and thermal properties, graphene is recognized as one of the most promising materials in research areas [18]. Nowadays, there have been a variety of researches focused on the electronic structure and quantum transport of grapheme [19–21]. Furthermore, fabrication of novel nanocomposites and devices based on graphene or graphene oxide

* Corresponding author. Tel.: +86 512 62872629; fax: +86 512 62603079.
** Corresponding author at: Department of Physics, University of Science and Technology of China, Hefei, Anhui 230026, PR China. Tel.: +86 551 3607090; fax: +86 551 3606266.
E-mail addresses: tkong2009@sinano.ac.cn (T. Kong), xpwang@ustc.edu.cn (X. Wang).

0039-9140/$ – see front matter © 2011 Elsevier B.V. All rights reserved.
doi:10.1016/j.talanta.2011.12.054

(GO) are also considered to be another hot spot [22–24]. Seger et al. used GO–Pt to build a fuel cell and showed that the graphene, as an efficient carrier of electrocatalyst, can improve the electrocatalytic activity of the fuel cell [25]. Paek et al. constructed a lithium battery by SnO_2/graphene nanosheet and found that the graphene can act as an effective conductive channel to enhance the electrochemical performances [26].

In this work, we synthesized reduced graphene oxide/Fe_3O_4 nanocomposite (NC_{RGO/Fe_3O_4}) by coprecipitation method. Then, a non-enzymatic hydrogen peroxide sensor was constructed based on the mimetic enzyme property of Fe_3O_4 nanoparticles (NPs) and RGO. Its catalytic properties were investigated in detail. The fabricated sensor showed a good integrated performance with wide linear range, fast response time and low detection limit.

2. Materials and methods

2.1. Reagents and chemicals

Hydrogen peroxide (30%), ferric chloride hexahydrate and ammonia solution (25%) were purchased from Sinopharm Chemical Reagent Co., Ltd. Phosphate buffered saline solution (PBS), ferrous chloride and chitosan were purchased from Shanghai Sangon Biological Engineering Technology & Services Co., Ltd. The deionized (DI) water ($R \geq 18.2\,M\Omega\,cm$) used in all experiments was produced by a Millipore system.

2.2. Synthesis of Fe_3O_4 NPs and RGO/Fe_3O_4 nanocomposites

Graphene oxide (GO) was synthesized from graphite powder based on modified Hummers method [27]. The GO was then treated with NaOH as follows. 10 mg GO was dispersed in 15 mL DI assisted by low power ultrasound. 0.5 mL of 1 M (mol/L) NaOH was added into the clarified GO solution for 60 min. The above solution was then dialyzed till it turned to be neutral, followed by dilution to 30 mL.

NC_{RGO/Fe_3O_4} was prepared by coprecipitation of Fe^{2+} and Fe^{3+} in the presence of GO in alkaline solution [28]. 15 mL as-prepared GO solution was purged with high purity nitrogen (99.999%) for 60 min in a 50 mL round-bottom flask. 2.5 mL iron source solution (containing 6.0 mg $FeCl_3{\cdot}6H_2O$ and 9.5 mg $FeCl_2{\cdot}4H_2O$) was added into the flask with vigorous stir under nitrogen atmosphere for 7 h. Subsequently, 1.5 mL of 1.5 M NH_4OH solution was introduced dropwise to precipitate the iron oxides. Afterwards, the solution was heated to 65 °C and maintained for 2.5 h. The black precipitate acquired in this step was the nanocomposites of RGO and Fe_3O_4 NPs. Finally, the nanocomposites were thoroughly washed with DI water for 3 times to remove excessive reagents.

Fe_3O_4 nanoparticles were prepared by the chemical coprecipitation method according to the reported literature with slight modifications [29]. 15 mL DI water was heated up to 65 °C under nitrogen atmosphere, and then 2.5 mL ion source solution was added into the DI water for 5 min under vigorous stir. During the above process, 2 mL of 1.5 M NH_4OH aqueous solution was added dropwise. It can be observed that the color of the solution gradually turned to black due to the formation of Fe_3O_4 nanoparticles. After the reaction, the Fe_3O_4 nanoparticles were also collected and washed for 3 times with DI water.

2.3. Modification of the electrochemical electrodes

The working electrode was a gold electrode composed of 200 nm RF sputtered Au film on a silicon wafer (2 mm × 2 mm), which was used in our previous work [30]. 0.3 mL NC_{RGO/Fe_3O_4} solution and 0.1 mL 2% (w/w) chitosan acetic acid solution were first thoroughly mixed. 2 μL of above mixture was dropped onto the cleaned working electrode and dried in air for overnight. The electrode was then washed with PBS to remove the unimmobilized NC_{RGO/Fe_3O_4} prior to use. For comparison, electrodes with only RGO or Fe_3O_4 nanoparticles and the mixture of RGO and Fe_3O_4 nanoparticles (M_{RGO/Fe_3O_4}) were also prepared with above similar procedure. The modified electrodes were stored at room temperature (typically, 25 °C) when not in use.

2.4. Sensor characterizations and electrochemical measurements

The morphology and structure of NC_{RGO/Fe_3O_4} were characterized by high-resolution transmission electron microscopy (HRTEM, JEOL-2010, Japan), scanning electron microscopy (SEM, JEOL-6700, Japan), and X-ray diffraction (XRD, D/Max-rA with Cu Kα of 1.54056 Å, Japan). Cyclic voltammetric and amperometric experiments were performed with a CHI 660A electrochemical workstation (Shanghai Chenhua Instruments Co., China). A conventional three-electrode system was adopted, in which the modified Au electrode, a platinum wire and a saturated calomel electrode (SCE) were served as working electrode, counter electrode and reference electrode, respectively. The cyclic voltammograms (CV) were recorded in 10 mL of pH 7.0 PBS at a scan rate of 0.1 V/s. The amperometric response of the fabricated sensor to H_2O_2 was collected in stirring (600 rpm) PBS at −0.3 V versus SCE. The solutions used in all electrochemical experiments were deaerated with nitrogen for 15 min before measurements. All electrochemical experiments were performed at room temperature.

3. Results and discussion

3.1. Characterizations of Fe_3O_4 NPs-decorated graphene

The morphology and structure of NC_{RGO/Fe_3O_4} were characterized by TEM, HRTEM and XRD, as shown in Fig. 1. It can be observed that the RGO sheet was about several micrometers in size and the Fe_3O_4 NPs were well dispersed on the surface of RGO (Fig. 1A). The diameter of Fe_3O_4 NPs on RGO was uniform and in the range of 35–45 nm, as shown in Fig. 1B. Furthermore, the HRTEM image of the Fe_3O_4 NPs in Fig. 1C illustrates that the NPs are of single-crystalline structure with no obvious defects. The interplanar spacings are measured to be 0.26 and 0.29 nm, corresponding to the lattice plane distance values of (3 1 1) and (2 2 0) planes of face-centered cubic (f.c.c.) Fe_3O_4, respectively. Fig. 1D shows the XRD pattern of NC_{RGO/Fe_3O_4} on Si substrate. The peak at $2\theta = 28.4°$ ($d = 0.3141$ nm) is assigned as the Si substrate (1 1 1) (JCPDS Card No. 03-0529). All the other peaks are identical with f.c.c. Fe_3O_4 (JCPDS Card No. 86-1361). The strong and sharp peaks indicate that the as-prepared samples were well crystallized, without any impurity phase.

3.2. Electrocatalytic activity of NC_{RGO/Fe_3O_4} electrode

To investigate the electrocatalytic activity of the NC_{RGO/Fe_3O_4} modified electrode, cyclic voltammetry (CV) was employed over a potential ranging from −0.8 to +0.8 V at a scan rate of 0.1 V/s in pH 7.0 PBS. Fig. 2 exhibits the CV curves of NC_{RGO/Fe_3O_4} modified electrode in the absence and presence of H_2O_2 in 10 mL PBS. For comparison, the electrochemical behavior of the RGO, Fe_3O_4 NP and M_{RGO/Fe_3O_4} modified electrodes are shown in Fig. S1 of the Supporting Information. It can be seen in Fig. 2 that a pair of well-defined redox peaks are observed on the NC_{RGO/Fe_3O_4} modified electrode. With addition of H_2O_2, the CV curve of the NC_{RGO/Fe_3O_4} modified electrode changes dramatically with an increase of reduction current, revealing an obvious electrocatalytic behavior to the reduction of H_2O_2. Meanwhile, as the concentration of H_2O_2 increases, the

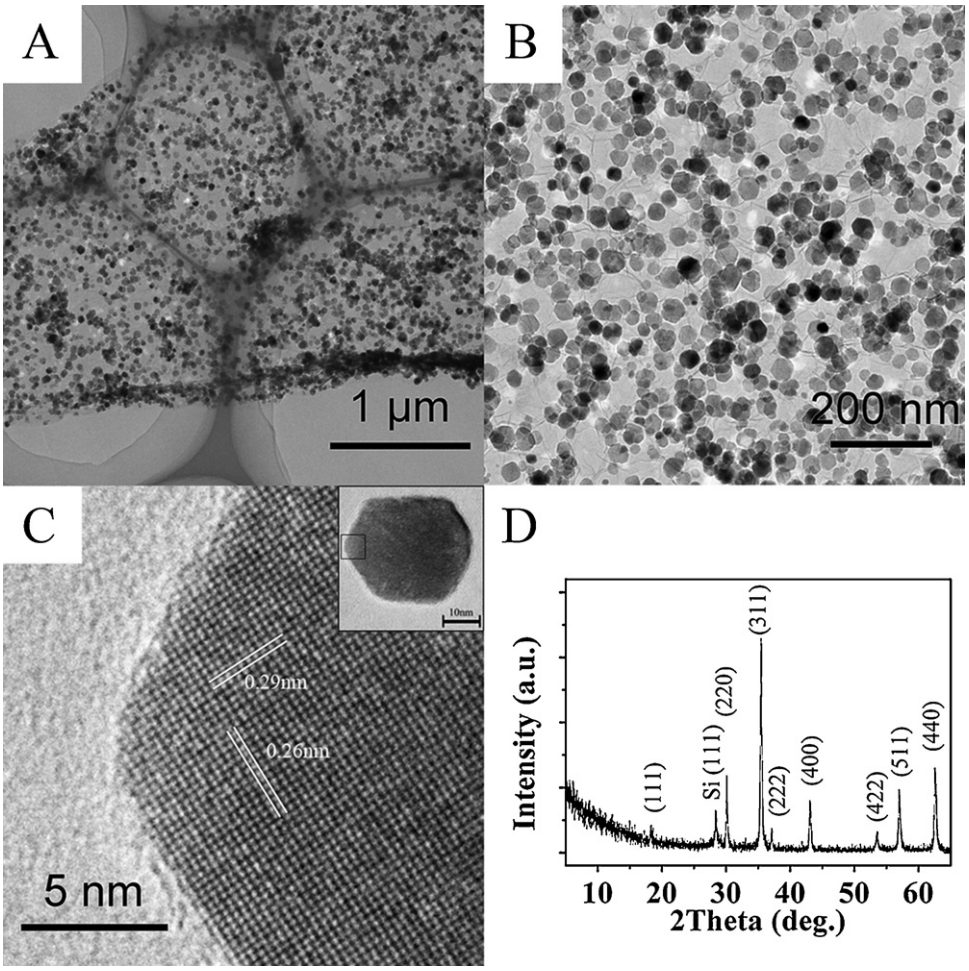

Fig. 1. Low-magnification (A) and high-magnification (B) TEM images, HRTEM (C) and XRD pattern (D) of the as-prepared NC_{RGO/Fe_3O_4}.

reduction current enhances correspondingly. However, in the cases of RGO, Fe_3O_4 NP and M_{RGO/Fe_3O_4} modified electrodes, no apparent redox peaks can be witnessed and higher potentials to reduce H_2O_2 are also needed. The reduction currents of these electrodes are also quite small compared with that of NC_{RGO/Fe_3O_4}. These results suggest that the NC_{RGO/Fe_3O_4} modified electrode has good electrocatalytic ability to the electro-reduction of H_2O_2.

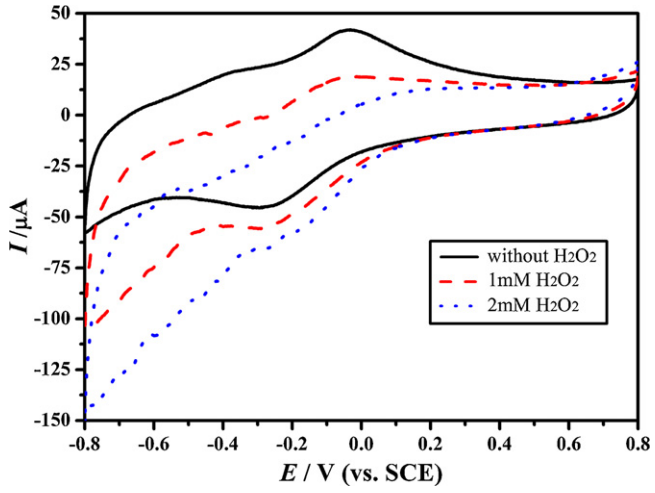

Fig. 2. Cyclic voltammograms of NC_{RGO/Fe_3O_4} modified electrode in the absence and presence of different concentrations of H_2O_2 in 10 mL pH 7.0 PBS at 0.1 V/s.

3.3. Response behavior of the H_2O_2 sensor

It is well known that the performance of a sensor is significantly affected by the applied working voltage. In this work, to determine an optimal voltage for the fabricated sensor, we first investigated the relationship between the response current and the applied voltage. As illustrated in Fig. S2 of the Supporting Information, the reduction current increases when the voltage is below −0.3 V and reaches a plateau till the voltage reaches at −0.6 V. Although the reduction current increases after −0.6 V, −0.3 V is still chosen for this work in order to prevent possible interference of electroactive species at high voltages.

Fig. 3 shows the amperometric response of NC_{RGO/Fe_3O_4} modified electrode at −0.3 V upon successive addition of H_2O_2. The current changes and reaches steady state rapidly when H_2O_2 is added into the PBS. The response time is less than 5 s. The inset of Fig. 3 shows the calibration curve of the response of the NC_{RGO/Fe_3O_4} modified electrode, it reveals that the electrode has a wide linear response to H_2O_2 ranging from 0.1 to 6 mM and a high sensitivity of 688.0 μA/mM cm^2, the linear regression equation is $I(mA) = -3.4 - 28.1 \times CH_2O_2(mM)$ ($R^2 = 0.990$) where I is the current and the CH_2O_2 is the H_2O_2 concentration. The limit of detection (LOD) is calculated to be 3.2 μM (signal–noise ratio of 3) according to previously published method [31].

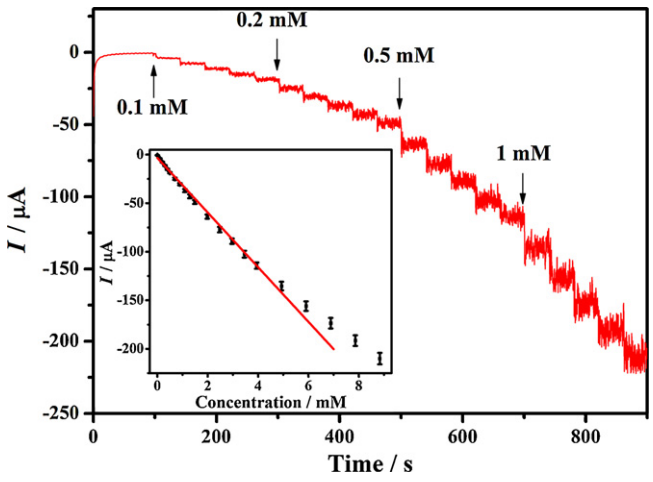

Fig. 3. Amperometric response and calibration curve (inset) of NC_{RGO/Fe_3O_4} modified electrode at −0.3 V upon successive additions of H_2O_2 into 10 mL PBS.

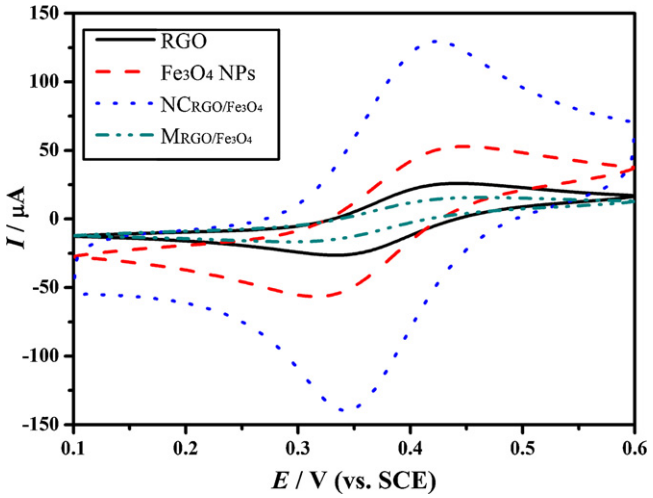

Fig. 4. The cyclic voltammograms of different materials modified electrodes in potassium ferricyanide solution at a scan rate of 50 mV/s.

Table 1 summarizes the sensitivity of different materials modified electrodes. The sensitivity of Fe_3O_4 NPs modified electrode is accordant with that of published work [16]. It can be found from Table 1 that the sensitivity of NC_{RGO/Fe_3O_4} modified electrode is much higher than that of RGO, Fe_3O_4 NPs or M_{RGO/Fe_3O_4}. We then discuss the mechanism of such enhancement as follows. Fe_3O_4 NPs possess the mimetic enzymatic property of H_2O_2 catalysis. The isoelectric point of Fe_3O_4 is around 5.9, which makes it positively charged in the chitosan solution. While the NH_4OH treated RGO is negatively charged. As a result, the electrostatic interaction dominates the combination of the RGO and Fe_3O_4 in the mixture (M_{RGO/Fe_3O_4}). Under the electrostatic interaction, the mixture is easy to aggregate as observed from Fig. S3 of the Supporting Information. However, as for the NC_{RGO/Fe_3O_4} synthesized by coprecipitation method, RGO and Fe_3O_4 NPs are combined tightly with little boundary defects which will facilitate the charge transfer between them and result in enhanced electrocatalytic ability to the reduction of H_2O_2.

We further performed an electrochemical experiment to verify the proposed mechanism. Potassium ferricyanide is commonly used in the electrochemical experiments to study the surface kinetics of the electrodes. It is reported that the smaller separation between peak potentials (ΔE_p) and larger peak current (I_p) of redox reaction indicate the larger kinetics on the electrodes [32]. As can be seen from Fig. 4, the NC_{RGO/Fe_3O_4} modified electrode possess the smallest ΔE_p and the largest I_p in contrast with the RGO, Fe_3O_4 NPs and M_{RGO/Fe_3O_4} modified electrode. This is the further evidence that RGO can promote the electron transfer in NC_{RGO/Fe_3O_4} to improve the sensitivity of the sensor.

3.4. Anti-interference performance, reproducibility and stability of the H_2O_2 sensor

The anti-interference ability is one of the most important analytical factors for a sensor. In this work, 0.1% fetal bovine serum (FBS), 2 mM of glucose (Glu), lactic acid (LA), ascorbic acid (AA), urea and 0.15 mM H_2O_2 were added into the PBS to investigate the anti-interference ability of the sensor. As seen from Fig. 5A,

Table 1
Comparison of the sensitivity of different materials modified electrodes to the electro-reduction of H_2O_2.

Electrode materials	RGO	Fe_3O_4 NP	M_{RGO/Fe_3O_4}	NC_{RGO/Fe_3O_4}
Sensitivity (μA/mM cm^2)	15.8	30.4	65.6	688

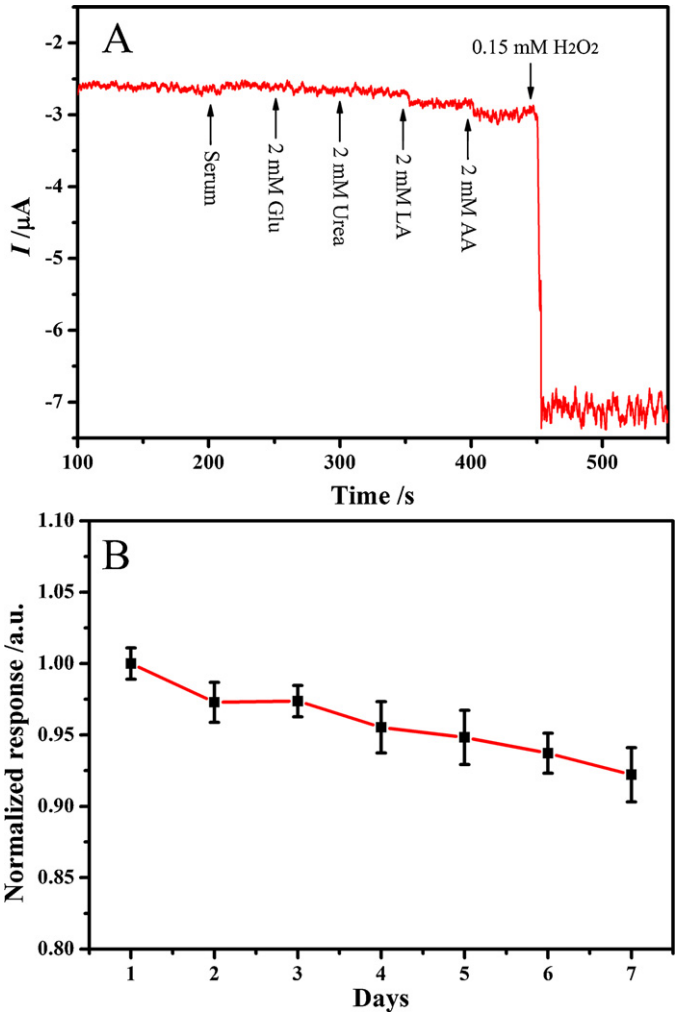

Fig. 5. Amperometric response to serum, glucose, urea, lactic acid, ascorbic acid and H_2O_2 of NC_{RGO/Fe_3O_4} modified electrode at −0.3 V in 10 mL PBS (A). Long-term stability of the constructed sensor (B).

Table 2
H_2O_2 level in real serum samples.

Sample	H_2O_2 added (mM)	H_2O_2 measured (mM)	Recovery (%)
1	0.1	0.105 ± 0.002	105.0
2	0.2	0.204 ± 0.01	102.0
3	0.3	0.317 ± 0.009	105.7

no obvious current changes after addition of serum, Glu and urea. However, 4.3% and 4.0% current increment can be observed when LA and AA are added, respectively. The effect of various inorganic salts including NaCl, KCl, $CaCl_2$, $MgCl_2$ and $Zn(NO_3)_2$ to the response of the sensor was studied as well, and the results are shown in Fig. S4. Only 4.1% current changes after addition of 2 mM $Zn(NO_3)_2$. Considering the concentration of interference species is much higher than that of H_2O_2, we conclude that the above species cause negligible effect for the H_2O_2 sensing and the NC_{RGO/Fe_3O_4} modified electrode has a quite good anti-interference performance.

The reproducibility and long-term stability of the NC_{RGO/Fe_3O_4} modified electrode are also evaluated. The relative standard deviation (R.S.D.) is 1.64% for three successive measurements. Four sensors fabricated independently give a R.S.D. of around 2.0% (Fig. S5). The long-term stability of the constructed sensor was examined by recording the current response to 0.5 mM H_2O_2 once a day. It was found that NC_{RGO/Fe_3O_4} modified electrode could retain 92% of initial response in one week as shown in Fig. 5B. All these data implies that the NC_{RGO/Fe_3O_4} modified electrodes possess good reproducibility and stability.

3.5. Detection of H_2O_2 in real sample

Real serum samples were utilized to demonstrate the practical usage of the fabricated H_2O_2 sensor. A series of serum sample containing H_2O_2 were tested and the results were listed in Table 2. As can be seen, the measured H_2O_2 concentrations are close to that of stoichiometrically added. This result suggests the suitability of the constructed H_2O_2 sensor in the matrix of serum.

4. Conclusions

In summary, a non-enzymatic hydrogen peroxide sensor based on the nanocomposite of reduced graphene oxide (RGO) and Fe_3O_4 NPs was developed. The modified electrode exhibited excellent catalytic activity to hydrogen peroxide. The biosensor displays rapid response, large linear range, low limit of detection, outstanding anti-interference ability and good reproducibility. Our results suggest that the RGO/Fe_3O_4 nanocomposite can be served as promising sensing elements in the construction of H_2O_2 sensors.

Acknowledgments

We acknowledge supports from Major State Basic Research Development Programs of China (2011CB921400) and National Natural Science Foundation of China (10874165, 90921013, 21121003, 20925311 and 11104317).

Appendix A. Supplementary data

Supplementary data associated with this article can be found, in the online version, at doi:10.1016/j.talanta.2011.12.054.

References

[1] K. Hirakawa, Anal. Bioanal. Chem. 386 (2006) 244–248.
[2] A. Tahirovic, A. Copra, E. Omanovic-Miklicanin, K. Kalcher, Talanta 72 (2007) 1378–1385.
[3] M.Y. Hua, H.C. Chen, C.K. Chuang, R.Y. Tsai, J.L. Jeng, H.W. Yang, Y.T. Chern, Biomaterials 32 (2011) 4885–4895.
[4] Y.H. Zhu, H.M. Cao, L.H. Tang, X.L. Yang, C.Z. Li, Electrochim. Acta 54 (2009) 2823–2827.
[5] L. Zhang, Biosens. Bioelectron. 23 (2008) 1610–1615.
[6] J.Q. Hu, Y. Yu, H.A. Guo, Z.W. Chen, A.Q. Li, X.M. Feng, B.M. Xi, G.Q. Hu, J. Mater. Chem. 21 (2011) 5352–5359.
[7] U. Jeong, X. Teng, Y. Wang, H. Yang, Y. Xia, Adv. Mater. 19 (2007) 33–60.
[8] H.M. Song, Q. Wei, Q.K. Ong, A. Wei, ACS Nano 4 (2010) 5163–5173.
[9] D. Tang, R. Yuan, Y. Chai, Anal. Chem. 80 (2008) 1582–1588.
[10] J.S. Choi, H.J. Choi, D.C. Jung, J.H. Lee, J. Cheon, Chem. Commun. (2008) 2197–2199.
[11] J.C. Frias, Y.Q. Ma, K.J. Williams, Z.A. Fayad, E.A. Fisher, Nano Lett. 6 (2006) 2220–2224.
[12] M.C. Urbina, S. Zinoveva, T. Miller, C.M. Sabliov, W.T. Monroe, C.S.S.R. Kumar, J. Phys. Chem. C 112 (2008) 11102–11108.
[13] L.Z. Gao, J. Zhuang, L. Nie, J.B. Zhang, Y. Zhang, N. Gu, T.H. Wang, J. Feng, D.L. Yang, S. Perrett, X. Yan, Nat. Nanotechnol. 2 (2007) 577–583.
[14] H. Wei, E. Wang, Anal. Chem. 80 (2008) 2250–2254.
[15] C. Zou, Y.C. Fu, Q.J. Xie, S.Z. Yao, Biosens. Bioelectron. 25 (2010) 1277–1282.
[16] M.S. Lin, H.J. Len, Electroanalysis 17 (2005) 2068–2073.
[17] G. Zhao, J.J. Feng, Q.L. Zhang, S.P. Li, H.Y. Chen, Chem. Mater. 17 (2005) 3154–3159.
[18] S. Gilje, S. Han, M. Wang, K.L. Wang, R.B. Kaner, Nano Lett. 7 (2007) 3394–3398.
[19] K.S. Novoselov, A.K. Geim, S.V. Morozov, D. Jiang, M.I. Katsnelson, I.V. Grigorieva, S.V. Dubonos, A.A. Firsov, Nature 438 (2005) 197–200.
[20] A.H. Castro Neto, F. Guinea, N.M.R. Peres, K.S. Novoselov, A.K. Geim, Rev. Mod. Phys. 81 (2009) 109.
[21] Y. Zhang, Y.-W. Tan, H.L. Stormer, P. Kim, Nature 438 (2005) 201–204.
[22] D.W. Choi, D.H. Wang, V.V. Viswanathan, I.T. Bae, W. Wang, Z.M. Nie, J.G. Zhang, G.L. Graff, J. Liu, Z.G. Yang, T. Duong, Electrochem. Commun. 12 (2010) 378–381.
[23] S.L. Chou, J.Z. Wang, M. Choucair, H.K. Liu, J.A. Stride, S.X. Dou, Electrochem. Commun. 12 (2010) 303–306.
[24] S. Watcharotone, D.A. Dikin, S. Stankovich, R. Piner, I. Jung, G.H.B. Dommett, G. Evmenenko, S.E. Wu, S.F. Chen, C.P. Liu, S.T. Nguyen, R.S. Ruoff, Nano Lett. 7 (2007) 1888–1892.
[25] B. Seger, P.V. Kamat, J. Phys. Chem. C 113 (2009) 7990–7995.
[26] S.M. Paek, E. Yoo, I. Honma, Nano Lett. 9 (2008) 72–75.
[27] W.S. Hummers, R.E. Offeman, J. Am. Chem. Soc. 80 (1958) 1339.
[28] L. Mao, R. Yuan, Y. Chai, Y. Zhuo, X. Yang, S. Yuan, Talanta 80 (2009) 1692–1697.
[29] F. Vereda, J. de Vicente, R. Hidalgo-Alvarez, Langmuir 23 (2007) 3581–3589.
[30] T. Kong, Y. Chen, Y.P. Ye, K. Zhang, Z.X. Wang, X.P. Wang, Sens. Actuators B 138 (2009) 344–350.
[31] M.P. O'Halloran, M. Pravda, G.G. Guilbault, Talanta 55 (2001) 605–611.
[32] X.M. Hou, L.X. Wang, F. Zhou, F. Wang, Carbon 47 (2009) 1209–1213.